International Journal of Solids and Structures xxx (xxxx) xxx

Contents lists available at ScienceDirect

International Journal of Solids and Structures

journal homepage: www.elsevier.com/locate/ijsolstr

# An explicit and accurate approach toward simulating plastic-to-pseudoelastic transitions of SMAs under multiple loading and unloading cycles

Lin Zhan[a], Xiao-Ming Wang[b], Si-Yu Wang[a,*], Hui-Feng Xi[a,*], Heng Xiao[a,c,*]

[a] School of Mechanics and Construction Engineering, MOE Key Lab of Disaster Forecast and Control in Engineering, Jinan University, West Huangpu Avenue 601, Guangzhou 510632, China
[b] Ningbo Polytechnic, Ningbo, China
[c] Shanghai Institute of Applied Mathematics and Mechanics, Shanghai University, Yanchang Road 149, Shanghai 200072, China

ARTICLE INFO

*Article history:*
Received 28 January 2019
Revised 21 June 2019
Accepted 19 August 2019
Available online xxx

*Keywords:*
Shape memory alloys
Plasticity
Pseudo-elasticity
Loading cycles
Continuous transitions
Explicit simulation

ABSTRACT

New finite elastoplastic $J_2$-flow equations are proposed for the purpose of explicitly simulating continuous transitions from plastic to pseudo-elastic effects of SMAs under multiple loading-unloading cycles. Novelties of such models are as follows: (i) New hardening effects are incorporated by introducing interplay between the changing of the yield surface radius and the moving of the yield surface center; (ii) extensive experimental data may be accurately simulated for any given number of loading-unloading cycles; (iii) the complicated task for simulating extensive data may be accomplished by independently fitting certain single-variable functions; and (iv) such single-variable functions may be presented in explicit forms for the purpose of automatically, accurately fitting extensive data, thus bypassing uncertainties and undue complexities usually involved in iteratively solving a coupled system of nonlinear constitutive rate equations toward identifying numerous unknown parameters.

Numerical examples for model validation are presented and in good agreement with stress-strain data up to 20 loading-unloading cycles given in literature.



## 1. Introduction

Because of their unique properties such as the shape memory effect and the pseudo-elastic effect, SMAs (shape memory alloys) are widely used in the fields of aerospace, automatic control and biomedical engineering, etc. For their effective applications it is of much significance to establish constitutive models for SMAs with such unique effects. To date numerous results have been obtained from various standpoints, as may be seen in the recent surveys (Patoor et al., 2006; Lagoudas et al., 2006; Lagoudas, 2008).

SMAs exhibit rich yet complicated deformation effects under different conditions. The pseudo-elastic effect with strain recovery and the plastic effect with permanent set may be successively induced at different deformation stages. Under cyclic loading conditions, transitions between these effects may be observed, as shown, e.g., in Shaw and Kyriakides (1995) and in Zaki and Moumni (2007).

In the past decades, constitutive models for plastic and pseudo-elastic effects of SMAs from various standpoints have been proposed under various conditions, especially under cyclic loadings. Attention is usually directed to the pseudo-elastic effect. Results prior to 2005 may be found in the foregoing survey articles. Certain recent studies after 2005 in phenomenological modeling of SMA pseudo-elasticity may be found, e.g., in Panico and Brinson (2007), Luig and Bruhns (2008), Hartl and Lagoudas (2009), Lagoudas et al. (2012), Baldelli et al. (2015), Dong et al. (2016), Cui et al. (2017), Hartl et al. (2018) and many others.

Representatives for results related to cyclic loading cases are briefly described as follows. A phenomenological model with three internal variables was suggested in Tanaka et al. (1995) to simulate the stress-strain and strain-temperature hysteresis loops for the cyclic uniaxial deformation of SMA samples. A generic Gibbs free energy for polycrystalline SMAs in the presence of plastic strain was presented in Bo and Lagoudas (1999a) based on the micro-mechanical representative volume element. This theory was further used and developed in modeling several respects of SMA behaviors, including some specific cases of thermally

* Corresponding authors.
*E-mail address:* xiaoheng@shu.edu.cn (H. Xiao).

https://doi.org/10.1016/j.ijsolstr.2019.08.024
0020-7683/

induced phase transformation under varying magnitude of applied load (Lagoudas and Bo, 1999), the evolution of plastic strain etc. (Bo and Lagoudas, 1999b), as well as the minor hysteresis loops under cyclic loading (Bo and Lagoudas, 1999c). In Abeyaratne and Kim (1997), one more internal variable was introduced to study a variety of phenomena under cyclic loadings. On the other hand, three new internal variables were introduced in Zaki and Moumni (2007) to model SMA stress-strain and strain-temperature behaviors under cyclic loadings. Moreover, a super-elastic model for shape memory alloys was established in Saint-Sulpice et al. (2009) to describe the evolution of permanent inelastic strain in cyclic processes. Most recently, buckling and recovery of NiTi tubes under axial compression has been studied in Jiang et al. (2016a,b). Also, recent results in the respect of SMA plasticity and transformation may be found in Auricchio et al. (2007), Hartl et al. (2010), Morin et al. (2011a,b), Zhou (2012), Ashrafi et al. (2016) and many others.

Usually, plastic effects and pseudo-elastic effects need be separately characterized by introducing a number of additional internal variables related to micro-mechanisms, such as phase fractions, detwinning and martensite re-orientation etc. For these purposes several class of models should be introduced either from the micro-structural standpoint or from the phenomenological standpoint. Micromechanism-based models are known to be predictive while the identification of their parameters might be challenging. On the other hand, purely phenomenological models do not have this prediction capability. As a rule, a number of relevant criteria for phase changes should be assumed on an ad hoc basis. This situation would further be complicated by the following fact, viz., extensive experimental data need be fitted in simulating continuous plastic-to-pseudoelastic transitions under multiple loading cycles. Uncertainties and undue complexities would be involved in identifying many unknown parameters, as will be explained in Section 2. This may be the case even for a single loading und unloading cycle. As such, it does not appear that complete and accurate simulations of the foregoing transitions under multiple loading cycles could be achieved based on existing approaches.

The above issue will be addressed in this article. Extending the novel, direct approach proposed in a series of most recent studies (Xiao, 2013; 2014a; Wang et al., 2015; Xiao et al., 2016), we are going to propose new finite elastoplastic $J_2$−flow models for the purpose of simultaneously simulating both plastic and pseudo-elastic effects of SMAs. With this new model, a unified and explicit approach may be established toward accurately simulating continuous transitions from plastic to pseudo-elastic effects under any given number of loading and unloading cycles. Below are the main novelties of this study:

(i) New hardening effects are characterized by introducing interaction between the changing of the yield surface radius and the moving of the yield surface center;
(ii) Extensive experimental data may be accurately simulated for any given number of loading and unloading cycles;
(iii) The complicated task for simulating such extensive data may be accomplished by independently fitting certain single-variable functions; and
(iv) Such single-variable functions may be presented in explicit forms for the purpose of automatically, accurately fitting the foregoing extensive data, thus bypassing uncertainties and undue complexities usually involved in treating nonlinear constitutive rate equations toward identifying numerous unknown parameters.

Numerical examples for model validation will be presented and compared with test data in literature.

The main content of this article is arranged as follows. In Section 2, the main features of continuous transitions from plastic to pseudo-elastic effects will be described. In Section 3, a finite strain elastoplastic $J_2$−flow model with new hardening effects will be proposed and then this model will be shown to be thermodynamically consistent by presenting both the Helmholtz free energy function and the specific entropy function in explicit forms. In Section 4, responses of a uniaxial SMA sample under cyclic loading conditions will be taken into consideration and suitable single-variable functions are introduced to represent stress-strain curves at loading and unloading. In Section 5, multi-axial hardening moduli will be presented in explicit forms in terms of the introduced single-variable functions. In Section 6, numerical examples are presented and compared with test data for the purpose of model validation. Finally, in Section 7, the main novelties of the present study will be summarized and remarks are given for future development.

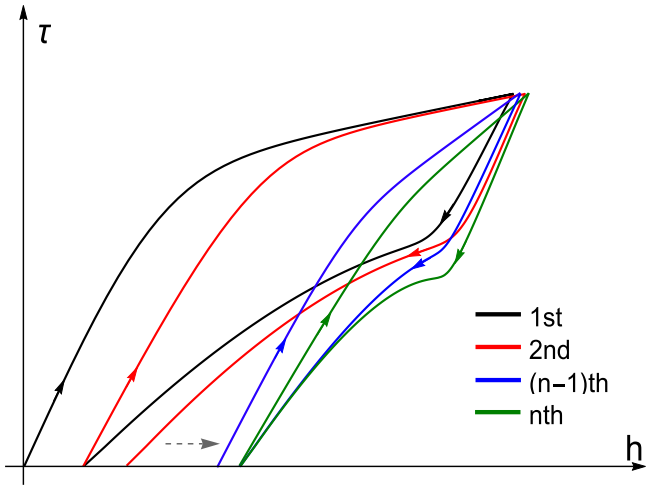


**Fig. 1.** Plastic-to-pseudoelastic transition of SMA sample under cyclic loading and unloading conditions.

## 2. Continuous transitions from plastic to pseudo-elastic effects

In this section, continuous transitions of SMA samples from plastic to pseudo-elastic effects will be described by means of macroscopic stress-strain responses under multiple loading and unloading cycles. In this respect, reference may be made to, e.g., Auricchio et al. (2007), Hartl and Lagoudas (2009), and Ashrafi et al. (2016) for discussions and results concerning plasticity and martensitic transformation.

Consider a uniaxial SMA sample subjected to $N$ successive loading-unloading cycles. At the $s$th cycle, this sample is loaded from zero to a given stress level and then unloaded to zero stress and, at the next cycle, i.e. the $(s+1)$th cycle, it is loaded from zero to another stress level and then again unloaded to zero stress. At the first cycle, an appreciable irrecoverable strain is induced. The irrecoverable strain induced in this cycling process goes monotonically down and becomes actually vanishing up to the $N$th cycle. During each cycle, a pair of stress-strain curves may be generated at loading and unloading, separately, and a gradual transition from plastic to pseudo-elastic effects may be induced from the 1st to the $N$th cycle, as schematically shown in Fig. 1.

Suppose that adequate stress-strain data are obtained from experimental tests for each loading and unloading cycle. Then, $N$ sets of such stress-strain data are available for the $N$ loading and unloading cycles at issue, which correspond with the $N$ pairs of stress-strain curves in Fig. 1. The objective for simulating the plastic-to-pseudoelastic transition as shown in Fig. 1 is as follows:

*Establish a suitable system of constitutive equations for SMAs, so that all the uniaxial stress-strain responses derived from this*

Please cite this article as: L. Zhan, X.-M. Wang and S.-Y. Wang et al., An explicit and accurate approach toward simulating plastic-to-pseudoelastic transitions of SMAs under multiple loading and unloading cycles, International Journal of Solids and Structures, https://doi.org/10.1016/j.ijsolstr.2019.08.024

*constitutive system for the N loading-unloading cycles at issue match as closely as possible any given N sets of stress-strain data for these loading-unloading cycles. In the meantime, such constitutive equations should be established for general multi-axial deformations and hence capable of predicting multi-axial responses.*

It might not be simple to arrive at the above objective under even a single cycle, let alone multiple cycles. Usually, simulation results at initial studies would be only roughly in agreement with test data. The main complexity lies in the fact that usually a number of unknown parameters should be introduced and have to be identified iteratively by means of trial-and-error procedures. This means that, for each possible set of trial values of the unknown parameters introduced, a coupled system of nonlinear rate type constitutive equations proposed should be solved toward obtaining all the uniaxial stress-strain responses for the *N* loading and unloading cycles. Such procedures should be carried out until a reasonable fit is attained.

Three issues would be left outstanding in the above procedures. In fact, there would be no certainties in arriving at a reasonable fit for given sets of data and, in particular, in ensuring accurate agreement. In fact, it may be expected that undue complexities would be involved in treating a coupled system of nonlinear constitutive rate equations with a number of unknown parameters.

In the subsequent development it will be shown that new finite strain elastoplastic $J_2-$flow equations may be established toward explicitly and accurately simulating gradual transitions from plastic to pseudo-elastic effects of SMAs under any given number of loading and unloading cycles. Toward this goal, extensive stress-strain data may be accurately, automatically simulated by simply providing certain single-variable functions fitting these data, thus bypassing the complicated issues in the foregoing.

## 3. New $J_2-$flow model with coupled hardening effects

In most recent studies, a new and direct approach has been proposed toward modeling deformation effects of SMAs, including the pseudo-elastic effects (Xiao et al., 2010a; 2010b; Xiao, 2013; 2014a; Wang et al., 2015) and the plastic effect etc. (Xiao et al., 2016). It has been demonstrated that all such effects may be simulated based simply on new elastoplastic $J_2-$flow models with nonlinear combined hardening. The central idea is to find out the hardening moduli incorporated in such new models, so that all the deformation effects of SMAs may be automatically, accurately simulated. In these recent works, results have been presented for cases of single pseudo-elastic hysteresis loops. As indicated before, here this new approach will further be developed for the purpose of simulating continuous transitions from plastic to pseudo-elastic effects under multiple loading and loading cycles. To this end, a new elastoplastic $J_2-$flow model should be proposed by developing the most recent models in the foregoing.

We direct attention to the self-consistent Eulerian rate formulation of finite elastoplastic deformations, as elaborated in Xiao et al. (2000a, 2000b, 2006, 2007). This formulation is based on the additive separation of stretching $\boldsymbol{D}$ into the elastic part $\boldsymbol{D}^e$ and the plastic part $\boldsymbol{D}^p$, viz.,

$$\boldsymbol{D} = \boldsymbol{D}^{\mathrm{e}} + \boldsymbol{D}^{\mathrm{p}} . \tag{1}$$

The constitutive equations governing the above two parts need be presented, as will be shown below, separately.

### 3.1. Self-consistent elastic rate equation

The elastic part $\boldsymbol{D}^e$ is governed by the following objective rate equation:

$$\begin{cases} \boldsymbol{D}^{\mathrm{e}} = \frac{\partial^2 \overline{W}}{\partial \boldsymbol{\tau}^2} : \overset{\circ}{\boldsymbol{\tau}} , \\ \overline{W} = \frac{1}{4G}\mathrm{tr}\boldsymbol{\tau}^2 - \frac{1}{4G}\frac{\nu}{1+\nu}(\mathrm{tr}\boldsymbol{\tau})^2 . \end{cases} \tag{2}$$

In the above, the $\boldsymbol{\tau} = J\boldsymbol{\sigma}$ is the Kirchhoff stress with $\boldsymbol{\sigma}$ and $J$ the true (Cauchy) stress and the volumetric ratio (the Jacobian), the $\overline{W}$ is the quadratic complementary elastic potential with the Poisson ratio $\nu$ and the shear modulus $G$, and the $\overset{\circ}{\boldsymbol{\tau}}$ is the co-rotational logarithmic rate of the Kirchhoff stress $\boldsymbol{\tau}$ (Xiao et al., 1997a; 1997b; 1997c). Generally, the logarithmic rate of a 2nd-order tensor $\boldsymbol{S}$, denoted $\overset{\circ}{\boldsymbol{S}}$, is defined as follows (Xiao et al., 1997a):

$$\overset{\circ}{\boldsymbol{S}} \equiv \dot{\boldsymbol{S}} + \boldsymbol{S}\cdot\boldsymbol{\Omega} - \boldsymbol{\Omega}\cdot\boldsymbol{S},$$

where $\boldsymbol{\Omega}$ is the logarithmic spin given in Xiao et al. (1997a, 1997b, 1997c). Throughout, $\dot{Z}$ represents the material time derivative of time-varying quantity $Z$ in a deforming body.

The elastic rate Eq. (2) is self-consistent in the sense that, prior to the yielding, i.e., $\boldsymbol{D}^p = \boldsymbol{O}$, it is exactly integrable to really deliver a hyper-elastic equation. Details may be found in the foregoing references.

### 3.2. Normality flow rule

Next, the plastic part $\boldsymbol{D}^p$ is governed by the normality flow rule below:

$$\boldsymbol{D}^{\mathrm{p}} = \xi \frac{\hat{f}}{u}\frac{\partial f}{\partial \boldsymbol{\tau}} . \tag{3}$$

In the above, the $\xi$ is the plastic indicator taking the values 1 and 0 at the loading case and the unloading case, as given below (cf., Bruhns et al., 2003 and Xiao et al., 2007):

$$\xi = \begin{cases} 1 & \text{for} \quad f = 0, \hat{f}/u \geq 0 , \\ 0 & \text{for} \quad f < 0 \text{ or } [f = 0, \hat{f}/u \leq 0] , \end{cases} \tag{4}$$

and, in addition, the $u$, $f$ and $\hat{f}$ are the plastic modulus, the yield function of von Mises type and the loading function. The first will be given slightly later, and the latter two are of the form:

$$\begin{cases} f = \frac{1}{2}\,\mathrm{tr}(\tilde{\boldsymbol{\tau}} - \boldsymbol{\alpha})^2 - \frac{1}{3}r^2 , \\ \hat{f} = \frac{\partial f}{\partial \boldsymbol{\tau}} : \overset{\circ}{\boldsymbol{\tau}} . \end{cases} \tag{5}$$

In the above, the $\tilde{\boldsymbol{\tau}}$ is the deviatoric part of the Kirchhoff stress $\boldsymbol{\tau}$, the $\boldsymbol{\alpha}$ is the back stress, and the $r$ is the yield limit. As usually known, the $r$ specifies the radius of the yield surface and describes the isotropic hardening effect, while the back stress $\boldsymbol{\alpha}$ prescribes the yield surface center and characterizes the anisotropic (kinematic) hardening effect. Generally, both the yield surface radius and the yield surface center are constantly changing with development of plastic flow, as shown below.

It has been demonstrated (Bruhns et al., 2005) that the normality flow rule Eq. (3) is derivable from a weakened form of Ilyushin's postulate, in which the factor $\hat{f}/u$ is obtained from the consistency condition of plastic flow (cf., Bruhns et al., 2003), i.e., $\dot{f}$, as given in Eq. $(5)_2$ and Eq. (10) later on.

### 3.3. Coupled hardening effects

Instead of the usual plastic work, for effective characterization of hardening effects it may be essential to use the effective plastic work $\vartheta$ given below (cf., e.g., Xiao, 2014b; Xiao et al., 2016) in the whole development:

$$\dot{\vartheta} = (\tilde{\boldsymbol{\tau}} - \boldsymbol{\alpha}) : \boldsymbol{D}^{\mathrm{p}} . \tag{6}$$

Toward simulating the pseudo-elastic effect, it is found (Xiao, 2013; 2014a; Wang et al., 2015; Xiao et al., 2016) that the yield limit $r$ should rely on both the effective plastic work $\vartheta$ and the magnitude of the back stress $\zeta$, namely,

$$\begin{cases} r = r(\vartheta, \zeta) , \\ \zeta = \sqrt{1.5\mathrm{tr}\boldsymbol{\alpha}^2} . \end{cases} \tag{7}$$

Please cite this article as: L. Zhan, X.-M. Wang and S.-Y. Wang et al., An explicit and accurate approach toward simulating plastic-to-pseudoelastic transitions of SMAs under multiple loading and unloading cycles, International Journal of Solids and Structures, https://doi.org/10.1016/j.ijsolstr.2019.08.024

The representation above may be new in two respects. On the one hand, the effective plastic work $\vartheta$, instead of the usual plastic work, is used. On the other hand, with dependence of the yield surface radius $r$ (cf., Eq. (6)) on the back stress $\boldsymbol{\alpha}$, coupled hardening effects are introduced with interplay between the changing of the yield surface radius and the moving of the yield surface center. It appears that such coupling effects would be absent in usual representations for combined hardening effects.

Moreover, the traceless back stress $\boldsymbol{\alpha}$ is governed by the following new nonlinear anisotropic hardening rule (Xiao, 2013; 2014a; 2014b; Wang et al., 2015; Xiao et al., 2016):

$$\overset{\circ}{\boldsymbol{\alpha}} = c\boldsymbol{D}^{\mathrm{p}} - \omega\dot{\vartheta}\,\boldsymbol{\alpha}\,, \tag{8}$$

with the Prager modulus $c$ and the hysteresis modulus $\omega$ below:

$$c = c(\vartheta,\zeta)\,,\quad \omega = \omega(\vartheta,\tilde{\boldsymbol{\tau}},\boldsymbol{\alpha})\,. \tag{9}$$

From certain consistency requirements it may be derived that both the $\overset{\circ}{\tilde{\boldsymbol{\tau}}}$ in Eq. (2) and the $\overset{\circ}{\boldsymbol{\alpha}}$ in Eq. (8) should be the corotational logarithmic rate (Xiao et al., 1997a; 1997b; 1997c). Details in this respect may be found in Xiao et al. (2000a, 2006, 2007).

It may be seen that the evolution equation Eq. (8) with Eqs. (5) and (9) is a substantial extension of the widely used Armstrong-Frederick equation. Here, again the effective plastic work $\vartheta$ (cf., Eq. (6)), instead of the usual plastic work (cf., Eq. (16) given later on), comes into play and, perhaps more essentially, both the Prager modulus $c$ and the hysteresis modulus $\omega$ therein are no longer constant (cf., Eq. (9)) but changing with development of plastic flow.

Eqs. (7)–(9) with the effective plastic work $\vartheta$ (cf., Eq. (6)) introduce new hardening effects with interplay between the yield surface radius and the yield surface center. Here, use of the effective plastic work $\vartheta$ instead of the usual plastic work $\kappa$ (cf., Eq. (16) later on) is essential. In fact, the $\vartheta$ is monotonically increasing with development of any plastic flow and has direct relevance to the thermodynamic intrinsic dissipation (cf., Eqs. (17)–(18) below), whereas this would not be the case for the $\kappa$.

### 3.4. The plastic modulus

For a general form of the yield function $f = f(\boldsymbol{\tau},\boldsymbol{\alpha},\vartheta)$, the plastic modulus $u$ in Eq. (3) is given by (cf., e.g., Xiao, 2014a; Xiao, 2014b)

$$u = -\frac{\partial f}{\partial\vartheta}\frac{\partial f}{\partial\boldsymbol{\tau}} : (\tilde{\boldsymbol{\tau}}-\boldsymbol{\alpha}) - \frac{\partial f}{\partial\vartheta} : \mathbb{H} : \frac{\partial f}{\partial\boldsymbol{\tau}}\,,$$

where

$$\mathbb{H} = c\mathbb{I} - (\boldsymbol{\tau}-\boldsymbol{\alpha})\otimes\boldsymbol{\alpha}$$

with $\mathbb{I}$ the 4th-order identity tensor. Hence, for the von Mises yield function $f$ in Eq. $(5)_1$, the plastic modulus $u$ is of the form (cf., Xiao, 2014a):

$$u = \frac{2}{3}c\,r^2 + \frac{4}{9}r^3r' - \frac{4}{9}\omega\,r^3\tilde{r}'\zeta + \frac{4}{9}\zeta^{-1}r^2\Lambda(1.5c\tilde{r}' - \zeta\omega r)\,. \tag{10}$$

Here and henceforth, the following notations are introduced:

$$\begin{cases} r' = \frac{\partial r}{\partial\vartheta},\ \tilde{r}' = \frac{\partial r}{\partial\zeta}\,, \\ \Lambda = \frac{3}{2r}(\tilde{\boldsymbol{\tau}}-\boldsymbol{\alpha}) : \boldsymbol{\alpha}\,. \end{cases} \tag{11}$$

### 3.5. Thermodynamic consistency

There emerge pronounced dissipation effects associated with deformation behaviors of SMAs. From a rigorous standpoint based upon universal thermodynamic principles, the second law in thermodynamics stipulates restrictions for realistic thermo-mechanical processes experienced by materials. It may be essential that a constitutive model simulating SMA deformation behaviors should be thermodynamically consistent, namely, should fulfill the restrictions stipulated by the second law, toward ensuring its physical reality and reasonableness. With this in mind, the thermodynamic consistency of the new model proposed need be examined, as will be done below.

Toward the above goal, we present the specific entropy function $\eta$ and the free energy function $\Phi$ in explicit forms and then demonstrate that these forms identically fulfill the second law with non-negative intrinsic dissipation, viz., the Clausius-Duhem inequality (cf., e.g., Xiao et al., 2007) below:

$$\boldsymbol{\tau} : \boldsymbol{D} - \dot{\Phi} - \eta\dot{T} - \frac{J}{T}\boldsymbol{q}\cdot\nabla T \geq 0 \tag{12}$$

for any given forms of the constitutive quantities incorporated in the proposed model. In the above, $T>0$ is the absolute temperature, $\boldsymbol{q}$ is the heat flux vector and $J$ is the deformation Jacobian (volumetric ratio).

Introducing a monotonically increasing quantity $\Gamma = \Gamma(\vartheta,T)$ by

$$\Gamma(0,T) = 0,\ \frac{\partial\Gamma}{\partial\vartheta} > 0\,, \tag{13}$$

we construct the specific entropy function $\eta$ and the Helmholtz free energy function $\Phi$ in explicit forms below:

$$\eta = -\frac{\partial\Phi}{\partial T} + \frac{\partial^2\overline{W}}{\partial\boldsymbol{\tau}\partial T} : \boldsymbol{\tau}\,, \tag{14}$$

$$\begin{cases} \Phi = \psi(T) - \Gamma(\vartheta,T) + \kappa + W\,, \\ W = \frac{\partial\overline{W}}{\partial\boldsymbol{\tau}} : \boldsymbol{\tau} - \overline{W}\,. \end{cases} \tag{15}$$

In the above, $\psi(T)$ is a temperature-dependent quantity representing the specific heat capacity, and the $\overline{W}$ is the complementary elastic potential given in Eq. (2). In a broad sense, here each elastic constant is regarded to rely also on the temperature $T$. Besides, the $\kappa$ is the usual plastic work specified by

$$\dot{\kappa} = \boldsymbol{\tau} : \boldsymbol{D}^{p}\,. \tag{16}$$

Hence, the thermodynamic intrinsic dissipation

$$\mathcal{D} = \boldsymbol{\tau} : \boldsymbol{D} - \dot{\Phi} - \eta\dot{T} \tag{17}$$

is given by

$$\mathcal{D} = \frac{\partial\Gamma}{\partial\vartheta}\,\dot{\vartheta} \geq 0 \tag{18}$$

with Eq. (13). Note here that the changing rate of the effective plastic work $\vartheta$ is always non-negative, namely, $\dot{\vartheta}\geq 0$. In fact, from Eqs. (3)–(6) it may be deduced that

$$\dot{\vartheta} = \begin{cases} \frac{2}{3}r^2\frac{\hat{f}}{u} \geq 0 & \text{for the loading case}\,, \\ 0 & \text{for the unloading case}\,. \end{cases}$$

since the factor $\hat{f}/u$ should be non-negative as indicated in Eq. (4) (cf., e.g., Xiao et al., 2007).

Hence, from the above and the fact that the heat flux $\mathbf{q}$ should be such that $-\mathrm{q}\cdot\nabla T > 0$, we deduce that the inequality Eq. (12) is identically fulfilled. Thus, it may be concluded that the proposed model is thermodynamically consistent for any given forms of the hardening quantities $r$, $c$ and $\omega$.

It is worthwhile to point out that the free energy given in Eq. (15) represents a broad case with no reference to the usual assumption concerning the recovered energy and the dissipated energy, etc. In fact, here the treatment of the Clausius-Duhem inequality is based on a new, general approach proposed in the recent development (Xiao et al., 2007; Xiao, 2014a; Xiao, 2014b).

Please cite this article as: L. Zhan, X.-M. Wang and S.-Y. Wang et al., An explicit and accurate approach toward simulating plastic-to-pseudoelastic transitions of SMAs under multiple loading and unloading cycles, International Journal of Solids and Structures, https://doi.org/10.1016/j.ijsolstr.2019.08.024

### 3.6. Main procedures for explicit approach

The new model proposed is characterized by three hardening quantities, including the yield limit $r$ (cf., Eq. (7)), the Prager modulus $c$ and the hysteresis modulus $\omega$ (cf., Eq. (9)). Forms of these quantities as functions of the effective plastic work and other variables are to be found. It has been demonstrated in a series of studies (Xiao, 2013; 2014a; Wang et al., 2015; Xiao et al., 2016) that explicit expressions for the three quantities $r$, $c$ and $\omega$ may be presented for the purpose of simulating pseudo-elastic effects and plastic effects for single loading and unloading cycles.

In the subsequent development, it will be further demonstrated that explicit expressions for the three hardening quantities $r$, $c$ and $\omega$ may be presented for the purpose of simulating gradual transition from plastic to pseudoelastic effects under any given number of loading and unloading cycles as shown in Fig. 1.

A substantially new approach need be introduced toward arriving at the above objective in dealing with extensive data generated from multiple loading and unloading cycles. The main procedures of this new approach are as follows:

(i) Introduce $N$ pairs of single-variable functions, called shape functions, which represent $N$ pairs of stress-strain curves for $N$ loading-unloading cycles;
(ii) Supply explicit expressions for the above shape functions which accurately fit stress-strain data given for the $N$ loading-unloading cycles at issue;
(iii) Obtain explicit expressions for $r$, $c$ and $\omega$ in terms of the above shape functions, so that the response of the proposed model under the $N$ loading and unloading cycles at issue can exactly reproduce the $N$ pairs of stress-strain curves represented just by the above shape functions; and
(iv) Extend the above expressions from uniaxial to general multi-axial cases, so that the established model is ready for treating multi-axial responses.

By means of the above procedures, a unified and explicit approach may be established for the purpose of accurately simulating continuous transitions from plastic to pseudo-elastic effects under multiple loading-unloading cycles and, in the meantime, for the purpose of treating multi-axial response. Details for the above procedures will be given in the next two sections, separately.

## 4. Shape functions for loading and unloading curves

The first two procedures indicated in Section 3.6 will be explained in this section. The main issue here is to introduce a pair of single-variable functions (shape functions) representing a pair of stress-strain curves of a SMA sample in a loading-unloading cycle. It does not appear that this issue may be trivial, since such shape functions should be introduced in such a manner that explicit results in the last two procedure in Section 3.6 can be obtained.

As schematically shown in Fig. 2, a loading curve $P_0P_1P_2$ with a linear part $P_0P_1$ and an unloading curve $P_2Q_1Q_2$ with a linear part $P_2Q_1$ are generated in a loading and unloading cycle. On this pair of loading and unloading curves locate five particular points, including the starting point of loading, $P_0$, the two initial yield points $P_1$ and $Q_1$ at loading and unloading, the starting point of unloading, $P_2$, and the finishing point of unloading, $Q_2$. The axial Kirchhoff stress, the axial Hencky (logarithmic) strain, and the effective plastic work at these five points in the $n$th cycle are designated by $P_0(0, h^p_{n-1}, \vartheta_n)$, $P_1(r_0,\ h_{0n},\ \vartheta_n)$, $P_2(\overline{\tau}^*_n, \overline{h}^*_n, \vartheta^*_n)$, $Q_1(\underline{\tau}^*_n, \underline{h}^*_n, \vartheta^*_n)$, and $Q_2(0, h^p_n, \vartheta^p_n)$, respectively. Moreover, the slopes of the two linear parts $P_0P_1$ and $P_2Q_1$ are given by the Young's modulus $E$.

The following relationships hold:

$$\begin{cases} \vartheta_n = \vartheta^p_{n-1}\,, \\ \vartheta^p_0 = 0\,, \end{cases} \tag{19}$$

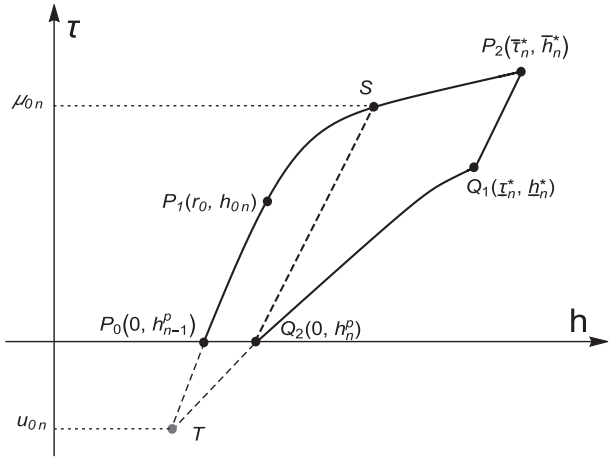


**Fig. 2.** Loading curve $P_0P_1P_2$ and unloading curve $P_2Q_1Q_2$ of a SMA sample generated from a loading and unloading cycle, with points $P_0$ and $Q_2$ on the strain axis for the start of loading and the end of unloading, points $P_1$ and $Q_1$ for the start of yielding, point $P_2$ for the start of unloading, and the intersecting point $T$ below the strain axis.

and

$$\begin{cases} h_{0n} = h^p_{n-1} + \tilde{E} r_0\,, \\ h^p_0 = 0\,. \end{cases} \tag{20}$$

Here and henceforth,

$$\tilde{E} = E^{-1}$$

with Young's modulus $E = 2G(1+\nu)$.

A departure from the unloading behavior of usual metals is shown in Fig. 2. In fact, for a SMA sample, only the linear part $P_2Q_1$ is elastic and reverse yielding emerges as from point $Q_1$ in an unloading process of removing the stress, whereas, for a usual metal sample, the entire unloading process is elastic without yielding. Details may be found later on in Section 5.1 and in Xiao et al. (2010a,b) and Xiao (2013, 2014a).

Stress-strain data from experimental tests should be given for the pair of curves in Fig. 2. Whenever test data for these two curves are available, it is a straightforward matter to reproduce these curves by means of two single-variable functions. Usually, this may be done by presenting the axial stress as functions of the axial strain. For our purpose, however, these two curves should be represented by other types of functions, as presented below.

In what follows, $\overline{h}$ and $\overline{\tau}$ are used to denote the axial Hencky strain and the axial Kirchhoff stress at a generic point on the loading curve, while $\underline{h}$ and $\underline{\tau}$ to designate the axial Hencky strain and the axial Kirchhoff stress at a generic point on the unloading curve.

### 4.1. Shape functions for loading curves

For the $n$th cycle, the stress-strain curve at loading is represented by two strain-stress functions. For the loading curve $P_0P_1P_2$ in Fig. 2, the linear part $P_0P_1$ prior to yielding is represented by

$$\begin{cases} \overline{h} = \tilde{E}\overline{\tau} + h^p_{n-1}\,, \\ 0 \le \overline{\tau} \le r_0\,, \end{cases} \tag{21}$$

and the plastic part $P_1P_2$ after yielding by

$$\begin{cases} \overline{h} = p_n(\overline{\tau}),\ \overline{\tau} \ge r_0\,, \\ p_n(r_0) = h^p_{n-1} + \tilde{E} r_0\,. \end{cases} \tag{22}$$

Please cite this article as: L. Zhan, X.-M. Wang and S.-Y. Wang et al., An explicit and accurate approach toward simulating plastic-to-pseudoelastic transitions of SMAs under multiple loading and unloading cycles, International Journal of Solids and Structures, https://doi.org/10.1016/j.ijsolstr.2019.08.024

### 4.2. Shape functions for unloading curves

Next, the linear part $P_2Q_1$ in Fig. 2 is represented by

$$\begin{cases} \underline{h} = \overline{h}_n^* + \tilde{E}\big(\underline{\tau} - \overline{\tau}_n^*\big), \\ \underline{\tau}_n^* \le \underline{\tau} \le \overline{\tau}_n^*, \end{cases} \tag{23}$$

and the curve $Q_1Q_2T$ by

$$\begin{cases} \underline{h} = q_n(\underline{\tau}) = p_n(b_n\underline{\tau} + \mu_{0n}) - p_n(\mu_{0n}) + \tilde{E}(1-b_n)\underline{\tau} + h_n^p, \\ 0 \le \underline{\tau} \le \underline{\tau}_n^*. \end{cases} \tag{24}$$

In the above, $0 \le b_n \le 1$ is a dimensionless parameter, and $\mu_{0n}$ is the axial stress at point $S$ (cf., Fig. 2) and will be determined later on.

Given a shape function $p_n(\overline{\tau})$ (cf., Eq. (22)) specifying a loading curve $P_1P_2$ in Fig. 2, the shape function $q_n(\underline{\tau})$ given in Eq. (24) uniquely prescribes an unloading curve consisting of two parts, namely, the curve $Q_1Q_2$ and an extended part from point $Q_2$ to the intersecting point $T$ below the strain axis in Fig. 2. It should be noted that, via an unloading procedure producing an elastic linear part, each point on the loading curve $P_1P_2$ is directly associated with a point on the two-part unloading curve just mentioned. For instance, ($P_1$, $T$), ($S$, $Q_2$) and ($P_2$, $Q_1$) are three such pairs of points. The stresses $\overline{\tau}$ and $\underline{\tau}$ at each such pair of points should be related by the yield conditions and therefore the relationship below may be derived (cf., Xiao, 2014a and Xiao et al., 2016):

$$\overline{\tau} = b_n\underline{\tau} + \mu_{0n}.$$

Hence, the unloading curve $Q_1Q_2T$ is generated by moving each point at the loading curve $P_1P_2$ to a new point according to the above linear relationship. For $b_n = 1$, the former is simply generated by a translation of the latter and this particular case has been treated in Xiao (2013). The general case with $b_n \neq 1$ has been studied in Xiao (2014a).

### 4.3. Shape functions accurately fitting data

Forms of the single-variable functions $p_n(\overline{\tau})$ and $q_n(\underline{\tau})$ in Eqs. (22) and (24), i.e., the shape functions for $N$ pairs of stress-strain curves, may be chosen to accurately fit test data given for $N$ loading and unloading cycles indicated in Section 2. In what follows, we are going to present an explicit expression for $p_n(\overline{\tau})$ which can automatically, accurately fit any given data set for the loading case. With this expression, an explicit expression for $q_n(\underline{\tau})$ is directly available, as given in Eq. (24).

The shape function $\overline{h} = p(\overline{\tau})$ for the loading curve may be given by means of a usual interpolating polynomial, which precisely fits a given set of stress-strain data below:

$$(\overline{\tau}_r, \overline{h}_r), \quad r = 0, 1, \cdots, S,$$

for the loading curve $P_0P_1P_2$ in Fig. 2. However, an interpolating polynomial may be unsatisfactory, since the Runge phenomenon of oscillatory nature may emerge at the end points. Spline functions over a number of subintervals may be given piecewise and advantageous but could not present a unified, smooth expression over the whole interval.

Toward bypassing the above issue, here a new approach is suggested to combine any given number of piecewise linear splines over a number of subintervals into a unified and smooth function over the entire interval. Such a smooth shape function in unified form is given below:

$$\begin{cases} \overline{h} = p_n(\overline{\tau}) = \frac{\overline{\tau}}{E}\phi_0(\overline{\tau}) + \sum_{r=1}^{S}\phi_r(\overline{\tau})\big[\overline{h}_{r-1} + A_r(\overline{\tau} - \overline{\tau}_{r-1})\big], \\ A_r = \frac{\overline{h}_r - \overline{h}_{r-1}}{\overline{\tau}_r - \overline{\tau}_{r-1}}, \quad r = 1, \cdots, S, \end{cases} \tag{25}$$

In the above, the $\phi_r(\overline{\tau})$ are $S$ smooth functions of localized nature and given by

$$\begin{cases} \phi_0(\overline{\tau}) = \frac{1}{2}\big[\tanh\lambda_0\big(\frac{\overline{\tau}}{r_0} + 1\big) - \tanh\lambda_0\big(\frac{\overline{\tau}}{r_0} - 1\big)\big], \\ \phi_S(\overline{\tau}) = \frac{1}{2}\big[\tanh\lambda_0\big(\frac{\overline{\tau}}{r_0} - \frac{\overline{\tau}_{S-1}}{r_0}\big) + 1\big], \\ \phi_r(\overline{\tau}) = \frac{1}{2}\big[\tanh\lambda_0\big(\frac{\overline{\tau}}{r_0} - \frac{\overline{\tau}_{r-1}}{r_0}\big) - \tanh\lambda_0\big(\frac{\overline{\tau}}{r_0} - \frac{\overline{\tau}_r}{r_0}\big)\big], \\ r = 1, \cdots, S-1. \end{cases} \tag{26}$$

In the above, $\lambda_0 = 10r_0$ is a large non-dimensionalized constant and, besides, the initial values $(\overline{\tau}_0, \overline{h}_0)$ at $r = 0$ and the end values $(\overline{\tau}_S, \overline{h}_S)$ at $r = S$ are given by $(r_0, h_{n-1}^p + r_0/E)$ and $(\overline{\tau}_n^*, \overline{h}_n^*)$, respectively.

Each function $\phi_r$ above actually takes the constant value 1 within the interval $[\overline{\tau}_{r-1}, \overline{\tau}_r)$ and goes rapidly down to vanish outside the just mentioned interval. As such, the new shape function given in Eqs. (24)–(26) not only retains all the features of the usual piecewise linear splines over the $S$ subintervals, but also supplies a unified and smooth expression over the entire interval. In particular, it can automatically, accurately fit any given set of stress-strain data for the loading curve $P_1P_2$ in Fig. 2, viz.,

$$p_n(\overline{\tau}_r) = \overline{h}_r, \quad r = 0, 1, 2, \cdots, S.$$

Moreover, each shape function $q_n(\underline{\tau})$ for each unloading curve $Q_1Q_2$ in Fig. 2 is given by Eq. (24) with two parameters $b_n$ and $\mu_{0n}$. Since the loading curve $P_1P_2$ intersects the elastic line $Q_2S$ at point $S$, we infer

$$p_n(\mu_{0n}) = \tilde{E}\mu_{0n} + h_n^p,$$

This gives rise to

$$\begin{cases} \mu_{0n} = \frac{h_n^p - \overline{h}_{m-1} + A_m\overline{\tau}_{m-1}}{A_m - \tilde{E}}, \\ \overline{h}_{m-1} - \tilde{E}\overline{\tau}_{m-1} \le h_n^p \le \overline{h}_m - \tilde{E}\overline{\tau}_m. \end{cases} \tag{27}$$

In the above, $\tilde{E}$ is given by the expression immediately following Eq. (20). Note here that the second expression in Eq. (27) determines the positive integer $m$.

### 4.4. Remarks on the unloading shape function

It follows from the above and Eq. (24) that only a single parameter, i.e., $b_n$, is left to be identified in fitting the test data for each loading and unloading cycle, as will be shown in Section 6. However, it should be pointed out that the form of the unloading shape function $q_n(\underline{\tau})$, given in Eq. (24), is obtained by simply replacing the variable $\overline{\tau}$ in the loading function $p(\overline{\tau})$ for the curve $P_1P_2$ with a suitable linear transformation of $\overline{\tau}$, as explained at the last paragraph of Section 4.2. Moreover, it should be noted that the elastic linear part $P_2Q_1$ specified by Eq. (23) need not exactly fit the test data at the beginning of the unloading, as will be seen in Fig. 4(a)–(d) in Section 6. Further remarks in these respects will be given in Section 7.

The parameter $b_n$ may be determined by a direct procedure. In fact, let $\overline{\zeta}_n$ and $\underline{\zeta}_n$ be the slopes of the two curves $P_1P_2$ and $Q_1Q_2$ at points $P_2$ and $Q_1$, respectively. Then, the following relationship may be derived:

$$b_n = \frac{\underline{\zeta}_n^{-1} - E^{-1}}{\overline{\zeta}_n^{-1} - E^{-1}}. \tag{28}$$

For the particular case when $P_1P_2$ and $Q_1Q_2$ are parallel to each other, we have $\overline{\zeta}_n = \underline{\zeta}_n$ and hence $b_n = 1$, which has been treated in Xiao (2013).

For each of any $N$ loading-unloading cycles as shown in Fig. 1, the shape functions given in Eqs. (21) and (25)–(26) exactly fit the loading data in a direct sense, and then the shape functions given in Eqs. (23) and (24) are used to fit the unloading data with the

Please cite this article as: L. Zhan, X.-M. Wang and S.-Y. Wang et al., An explicit and accurate approach toward simulating plastic-to-pseudoelastic transitions of SMAs under multiple loading and unloading cycles, International Journal of Solids and Structures, https://doi.org/10.1016/j.ijsolstr.2019.08.024

parameter $b_n$ prescribed by Eq. (28). These procedures are explicit in the sense that they are carried out independently for each of the $N$ cycles at issue.

## 5. Hardening quantities in explicit forms

The last two procedures in Section 3.6 will be addressed in this section. To this end, we are going to present explicit expressions for the three hardening quantities $c$, $\omega$ and $r$ in terms of the shape functions introduced in the last section, so that any given pairs of stress-strain curves indicated in Section 2 may be automatically reproduced as the predictions of the proposed model with these quantities presented. In doing so, we shall first obtain separate expressions for the three hardening quantities for the $N$ cycles, namely, such expressions will be derived for the $N$ subranges, $[\vartheta_n, \vartheta_{n+1}]$ with $n = 1, 2, \cdots, N$, and, then, unified and smooth expressions over the whole range will be presented by combining the $N$ expressions over the $N$ subranges. The main procedures in deriving the former are the same as those in a most recent study (Xiao, 2014a; Xiao et al., 2016). In what follows the main results will be directly given and details in deriving them are omitted and may be found in these references.

### 5.1. Reverse plastic flow at unloading

From a direct standpoint based on the elastoplastic deformation behavior, in this study a novel idea is introduced to model the complicated responses of a SMA sample under multiple loading and unloading cycles. As is well known for usual metals, no plastic flow will be induced in an unloading process of removing a tensile load, while a reverse yield point will emerge under a compressive load after unloading. The latter is related to the anisotropic hardening known as the Bauschinger effect. The more pronounced the anisotropic hardening, the closer to the strain axis the reverse yield point. In particular, the reverse yield point may stay above the strain axis as the anisotropic hardening becomes exceptionally pronounced. This implies that reverse plastic flow may be induced just in an unloading process of removing a tensile load. In such an exceptional case, reverse plastic flow at unloading with much lower tangent moduli will give rise to much more pronounced strain recovery effect than the usual elastic unloading with very high Young's modulus. With this understanding, it is realized here that SMA deformation behaviors would just supply noticeable examples for such exceptional anisotropic hardening effects.

The above understanding may provide a perhaps new explanation of SMA deformation effects from a direct phenomenological standpoint. As shown in Fig. 2, a departure from the unloading behavior of usual metals is as follows: For a SMA sample, reverse yielding emerges as from point $Q_1$ in an unloading process of removing the stress above the strain axis, whereas, for a usual metal sample, the entire unloading process is elastic without yielding.

It is with the above new idea that the elastoplastic $J_2$−flow model has been proposed for modeling SMA deformation effects in Section 3. In what follows, we are going to show that the three hardening quantities $r$, $c$ and $\omega$, incorporated in the proposed model in Section 3, are obtainable in explicit forms, in the sense of exactly reproducing the $N$ pairs of shape functions introduced in the last section and, consequently, the proposed model with these hardening quantities can automatically match test data given for the $N$ pairs of stress-strain curves under a cyclic process consisting of $N$ cycles. Namely, any given pairs of stress-strain curves indicated in Section 2 may be automatically reproduced as the predictions of the proposed model with these hardening quantities.

Toward the above objective, we shall first obtain expressions for the three hardening quantities for $N$ cycles, separately. Specifically, such expressions will be derived for $N$ subranges of $\vartheta$, i.e., $[\vartheta_n, \vartheta_{n+1}]$ with $n = 1, 2, \cdots, N$, which demarcate the $N$ cycles at issues, and, then, unified smooth expressions over the whole range will be presented by a new approach of combining the $N$ expressions over the $N$ subranges into a single unified, smooth expression for each hardening quantity.

Results will be derived by means of three procedures below: (i) two equations will be derived from the proposed model for the uniaxial plastic flow curves $P_1P_2$ and $Q_1Q_2$, separately; (ii) these two uniaxial equations will be extended to a unified equation for general multiaxial cases; and (iii) three multiaxial hardening quantities will be obtained from this unified equation.

### 5.2. Results for individual cycles

For each cycle, either the loading curve or the unloading curve after the initial yield point represents a process of uniaxial plastic flow. For these uniaxial cases, the following two equations may be derived from the proposed model (Xiao, 2014a):

$$r'r - \omega r(\tilde{r}'\zeta + \Lambda) + 1.5c\zeta^{-1}\left(\zeta + \tilde{r}'\Lambda\right) = K(\tau) \tag{29}$$

where

$$K(\tau) = \begin{cases} \overline{K}(\overline{\tau}) & \text{along curve } P_1P_2 \text{ in Fig. 2}, \\ \underline{K}(\underline{\tau}) & \text{along curve } Q_1Q_2 \text{ in Fig. 2}, \end{cases} \tag{30}$$

with

$$\overline{K}(\overline{\tau}) \equiv \frac{1}{p'(\overline{\tau}) - \tilde{E}}, \tag{31}$$

$$\underline{K}(\underline{\tau}) \equiv \frac{1}{q'(\underline{\tau}) - \tilde{E}} = \frac{b^{-1}}{p'(b\underline{\tau} + r_0 - bu_0) - \tilde{E}} \tag{32}$$

are the plastic slopes (Xiao, 2014a; Xiao et al., 2016) for the loading curve and the unloading curve, respectively. As before, the following notation is used:

$$\tilde{E} = \frac{1}{E}.$$

Expressions for $c$ and $\omega$ are derivable from Eqs. (29)–(30), but such results are merely for the uniaxial case. As indicated in the last procedure in Section 3.6, however, results should be supplied for general multi-axial cases. Toward this objective, the two Eqs. (29)–(30) in the uniaxial case are extended to general multiaxial forms, namely (cf., Xiao, 2014a and Xiao et al., 2016),

$$r'r - \omega r(\tilde{r}'\zeta + \Lambda) + 1.5c\zeta^{-1}\left(\zeta + \tilde{r}'\Lambda\right) = K(r, \Lambda) \tag{33}$$

where

$$K(r, \Lambda) \equiv \frac{[r + \Lambda]}{r + |\Lambda|}\overline{K}(r + |\Lambda|) + \left(1 - \frac{[r + \Lambda]}{r + |\Lambda|}\right)\underline{K}(|\Lambda| - r), \tag{34}$$

with

$$[r + \Lambda] = \frac{1}{2}(r + \Lambda + |r + \Lambda|). \tag{35}$$

In the uniaxial case, Eq. (33) with Eqs. (34)–(35) automatically reduces to the two equations in Eq. (29) with Eqs. (30)–(32).

For $N$ pairs of loading and unloading curves as shown in Fig. 1, replacing the $r$, $p$, $u_0$ and $b$ in Eqs. (30)–(35) by $r_n$, $p_n$, $u_{0n}$ and $b_n$, from Eq. (33) we derive $N$ equations below:

$$\begin{cases} r_n'r_n - \omega_n r_n(\tilde{r}_n'\zeta + \Lambda_n) + 1.5c_n\zeta^{-1}\left(\zeta + \tilde{r}_n'\Lambda_n\right) = K_n(r_n, \Lambda_n), \\ n = 1, 2, \cdots, N, \end{cases} \tag{36}$$

for $N$ loading-unloading cycles.

If the quantities $r_n$, $c_n$ and $\omega_n$ for the $n$th cycle are given to meet the above equation, then the pair of loading and unloading curves shown in Fig. 2 may be automatically reproduced as the predictions of the proposed model.

Please cite this article as: L. Zhan, X.-M. Wang and S.-Y. Wang et al., An explicit and accurate approach toward simulating plastic-to-pseudoelastic transitions of SMAs under multiple loading and unloading cycles, International Journal of Solids and Structures, https://doi.org/10.1016/j.ijsolstr.2019.08.024

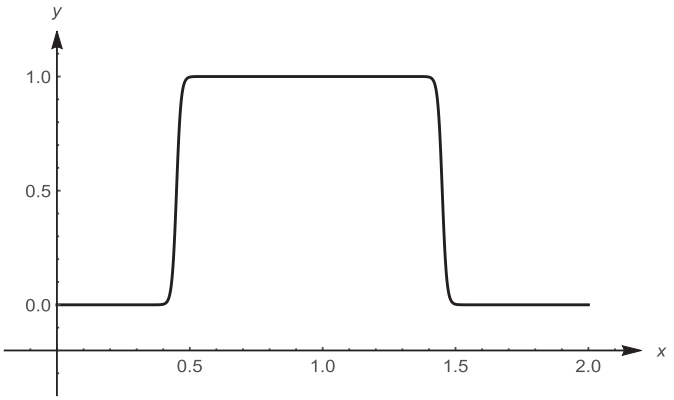


**Fig. 3.** The localized factor $y = \frac{1}{4}[1+\tanh(60(x-0.5)+3)][1+\tanh(60(1.5-x)-3)]$.

Following the procedures in (Xiao, 2014a; Xiao et al., 2016), we obtain $N$ pairs of explicit expressions for such quantities in terms of the $N$ shape functions $p_n(\overline{\tau})$ as follows:

$$c_n = \frac{2}{3}\frac{K_n(r_n, -\zeta\tilde{r}_n') - r_n r_n'}{1-\tilde{r}_n'^2}, \tag{37}$$

$$\omega_n r_n = 1.5\zeta^{-1}\tilde{r}_n' c_n + \frac{K(r_n, -\zeta\tilde{r}_n') - K_n(r_n, \Lambda_n)}{\Lambda_n + \tilde{r}_n'\zeta}. \tag{38}$$

On the other hand, the yield limits $r_n$ are given by

$$\begin{cases} r_1 = \frac{\mu_1}{b_1+1} + \frac{b_1-1}{b_1+1}\zeta\left(1-e^{-\varrho\frac{\zeta}{r_0}}\right) + \frac{r_0-\mu_1}{b_1+1}\left(e^{-\beta\frac{\vartheta}{r_0}} + e^{-\beta\frac{\vartheta_2-\vartheta}{r_0}}\right) \\ \qquad + \frac{b_1 r_0}{b_1+1}e^{-\beta\frac{\vartheta}{r_0}}, \\ r_n = \frac{\mu_n}{b_n+1} + \frac{b_n-1}{b_n+1}\zeta + \frac{r_0-\mu_n}{b_n+1}\left(e^{-\beta\frac{\vartheta-\vartheta_n}{r_0}} + e^{-\beta\frac{\vartheta_{n+1}-\vartheta}{r_0}}\right), \\ n = 2, \cdots, N. \end{cases} \tag{39}$$

In the above, $r_0$ is the initial yield limit and $\varrho > 0$ and $\beta > 0$ are two large parameters characterizing the localized properties at $\zeta = 0$ and $\vartheta = \vartheta_n, \vartheta_{n+1}$. In particular, the localized terms in Eq. (39) ensures the inter-cycle consistency, as shown below.

### 5.3. The inter-cycle consistency

Let $n \geq 2$ and consider the $n$th cycle as shown in Fig. 2. Point $P_0$ is the finishing point of the last cycle, i.e., the $(n-1)$th cycle. From the $(n-1)$th cycle it follows that both Eq. (39) for the $(n-1)$th cycle with omitting the localized effect and the yield condition produce

$$r_{n-1}^p = \frac{r_0}{b_{n-1}+1} + \frac{b_{n-1}-1}{b_{n-1}+1}\alpha_{n-1}^p,$$

$$\alpha_{n-1}^p = r_{n-1}^p,$$

where $r_{n-1}^p$ and $\alpha_{n-1}^p$ are the yield limit and the back stress at the end of the $(n-1)$th cycle.

On the other hand, the initial yielding in the $n$th cycle starts at point $P_1$ and both the yield limit and the back stress keep unchanged from $P_0$ to $P_1$ at the $n$th cycle. From these it may be inferred that the yield condition and Eq. (39) for the $n$th cycle with ignoring the localized effect yield

$$r_0 - \alpha_{n-1}^p = r_{n-1}^p,$$

$$r_{n-1}^p = \frac{r_0}{b_n+1} + \frac{b_n-1}{b_n+1}\alpha_{n-1}^p.$$

The above four expressions should be consistent with one another. In fact, it may be deduced that $r_{n-1}^p = \alpha_{n-1}^p = r_0/2$ and, therefore, that the consistency required is ensured.

The above derivation is for $n \geq 2$. The consistency for the first cycle may be directly shown with $r = r_0$ and Eq. $(39)_1$ at $\vartheta = 0$.

### 5.4. Effective plastic works

The effective plastic works at the end points of the $N$ cycles, i.e., $\vartheta_1, \cdots, \vartheta_N$, need be determined. This will be done below.

In the uniaxial loading case, the effective plastic work is given by

$$\dot{\vartheta} = (\overline{\tau} - \alpha)\dot{\overline{h^p}},$$

where $h^p$ is the axial plastic strain and prescribed by

$$\dot{\overline{h^p}} = \dot{h} - \tilde{E}\dot{\overline{\tau}}.$$

At any given point on the line $P_1P_2$ in Fig. 2, the yield condition yields

$$\overline{\tau} - \alpha = r_n.$$

Moreover, by neglecting the localized effects, Eq. (39) may be reduced to

$$r_n = \frac{b_n-1}{b_n+1}\alpha + \frac{r_0 - b_n u_{0n}}{b_n+1}.$$

The last two produce

$$r_n = \frac{1}{2b_n}((b_n-1)\overline{\tau} + r_0 - b_n u_{0n}) \tag{40}$$

along the curve $P_1P_2$ in Fig. 2. Similarly, it may be deduced that

$$r_n = \frac{1}{2}((b_n-1)\underline{\tau} + r_0 - b_n u_{0n}) \tag{41}$$

along the curve $Q_1Q_2$ in Fig. 2. In the uniaxial case, the effective plastic work $\vartheta$ is governed by

$$\dot{\vartheta} = \pm r(\dot{h} - \tilde{E}\,\dot{\tau}). \tag{42}$$

In the above, the signs "+" and "−" are for the curves $P_1P_2$ and $Q_1Q_2$, respectively. Hence, from Eqs. (24)–(26) and Eqs. (40)–(42) it follows that

$$\begin{cases} \vartheta_{n+1} = \vartheta_n + \frac{1}{4b_n}(A_m - \tilde{E})[(b_n-1)\overline{\tau}_m + \mu_n(b_n+1)](\overline{\tau}_m - \mu_n), \\ \qquad + \frac{1}{2b_n}\sum_{r=1}^{S}(A_r - \tilde{E})[(b_n-1)(\overline{\tau}_r + \overline{\tau}_{r-1}) + 2\mu_n](\overline{\tau}_r - \overline{\tau}_{r-1}), \\ \qquad - \frac{1}{4b_n}\sum_{r=1}^{m}(A_r - \tilde{E})[(b_n-1)(\overline{\tau}_r + \overline{\tau}_{r-1}) + 2\mu_n](\overline{\tau}_r - \overline{\tau}_{r-1}), \\ \vartheta_1 = 0, \quad n = 1, 2, \cdots, S-1, \end{cases} \tag{43}$$

where the $\mu_n$ is given by Eqs. (27)–(28).

### 5.5. Unified results for all cycles

Eqs. (37)–(39) provide $N$ explicit expressions for each of the three hardening quantities $c$, $\omega$ and $r$, which apply merely to the 1st, the 2nd, $\cdots$, the $N$th cycle, separately. Now the final step is to obtain unified expressions for $c$, $\omega$ and $r$ over the whole range, so that the foregoing $N$ expressions or values may be reproduced for the $N$ cycles, namely,

$$\begin{cases} c = c_n, \ \omega = \omega_n, \ r = r_n, \\ \vartheta_n \leq \vartheta < \vartheta_{n+1}, \\ n = 1, \cdots, N. \end{cases} \tag{44}$$

In the above, the $c_n$, $\omega_n$ and $r_n$ are the $N$ expressions piecewise given in the last subsection. As indicated at the outset of this section, the $\vartheta_n$ and $\vartheta_{n+1}$ are the values of the effective plastic work at the start of the $n$th and the $(n+1)$th cycle, respectively, and will be given in the next subsection

Here, a new method is proposed to obtain unified and smooth expressions of the above properties. With this new method, each

Please cite this article as: L. Zhan, X.-M. Wang and S.-Y. Wang et al., An explicit and accurate approach toward simulating plastic-to-pseudoelastic transitions of SMAs under multiple loading and unloading cycles, International Journal of Solids and Structures, https://doi.org/10.1016/j.ijsolstr.2019.08.024

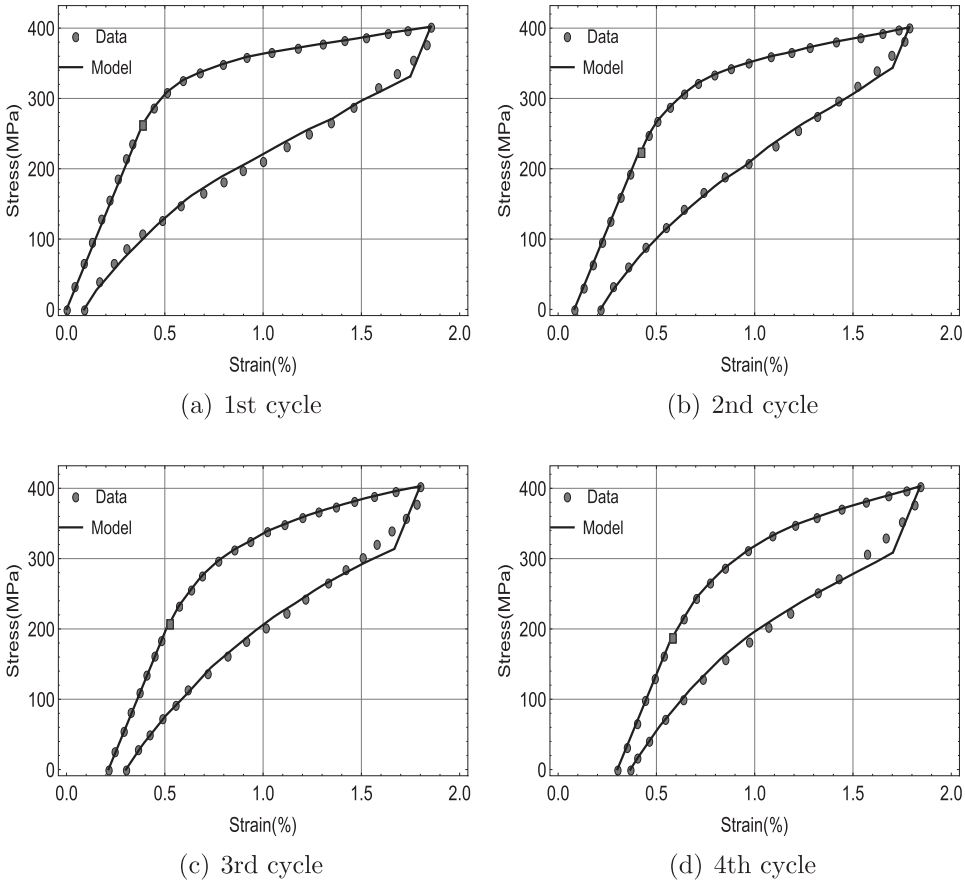


**Fig. 4.** Model simulations (solid lines) for the first four cycles and comparisons with test data (dots) in Zaki and Moumni (2007): The irrecoverable strain decreases with increasing cycle number.

unified expression will be obtained simply by a linear combination via a set of localized factors, i.e., $\varphi_1, \cdots, \varphi_N$, as given below:

$$c = \varphi_1 c_1 + \cdots + \varphi_N c_N, \tag{45}$$

$$\gamma = \varphi_1 \gamma_1 + \cdots + \varphi_N \gamma_N, \tag{46}$$

$$r = \varphi_1 r_1 + \cdots + \varphi_N r_N, \tag{47}$$

where

$$\varphi_n = \frac{1}{4}\left[1 + \tanh\left(60\frac{\vartheta - \vartheta_n}{\vartheta_{n+1} - \vartheta_n} + 3\right)\right] \times \left[1 + \tanh\left(60\frac{\vartheta_{n+1} - \vartheta}{\vartheta_{n+1} - \vartheta_n} - 3\right)\right]. \tag{48}$$

Each factor $\varphi_n = \varphi_n(\vartheta)$ given above is a smooth function over the whole range and of localized property, namely, it is nearly constant and given by 1 as $\vartheta$ falls within the range $[\vartheta_n, \vartheta_{n+1})$, whereas it goes rapidly down to vanish as $\vartheta$ falls outside the foregoing range. In fact, we have

$$\begin{cases} 0.9975 < \varphi_n < 1 \text{ for } \vartheta_n \le \vartheta \le \vartheta_{n+1} - 0.1(\vartheta_{n+1} - \vartheta_n), \\ 0 \le \varphi_n < 0.00245, \text{ for } \vartheta \le \vartheta_n - 0.1(\vartheta_{n+1} - \vartheta_n) \text{ or } \vartheta \ge \vartheta_{n+1}. \end{cases} \tag{49}$$

The above localized properties may be evidenced from Fig. 3 for a factor given by Eq. (48) over the subrange [0.5,1.5]. From these it may be deduced that the three quantities given in Eqs. (45)–(47) indeed meet Eq. (44).

Combining $N$ functions given over $N$ subranges via the $N$ factors in Eq. (48), Eqs. (45)–(47) supply unified, smooth expressions over the whole range, which exactly reproduce those functions (cf., Eq. (44)) over the $N$ subranges. It appears that the just indicated method of combining any given number of functions over subranges into a unified, smooth function over the whole range is proposed here for the first time.

### 5.6. Remarks

With the hardening quantities given here, the new model is established in the general framework of elastoplastic formulations with nonlinear combined hardening, as suggested in previous works (Xiao, 2013; 2014a). In this general framework, forms of the quantities characterizing both isotropic and anisotropic hardening, including the yield limit $r$ (cf., Eq. (6)) and the Prager modulus $c$ and the hysteresis modulus $\omega$ (cf., Eq. (9)), are left unknown and need to be determined. Forms of the just mentioned three hardening quantities are presented in previous works only for a single pseudo-elastic hysteresis loop involving one loading-unloading cycle. From the results given in the last section and in this section it may follow that the present work contributes perhaps substantially new results in the following respects:

(i) Any given number of loading-unloading cycles may be treated and explicit forms of the three hardening quantities $r$, $c$ and $\omega$ are derived for this broad case based on a novel approach, as indicated below;
(ii) New single-variable shape functions are presented in explicit forms for the purpose of automatically, accurately matching

Please cite this article as: L. Zhan, X.-M. Wang and S.-Y. Wang et al., An explicit and accurate approach toward simulating plastic-to-pseudoelastic transitions of SMAs under multiple loading and unloading cycles, International Journal of Solids and Structures, https://doi.org/10.1016/j.ijsolstr.2019.08.024

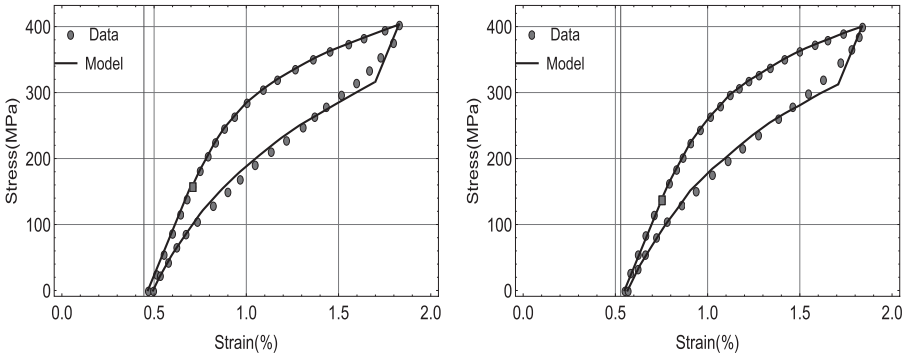


(a) 8th cycle (b) 12th cycle

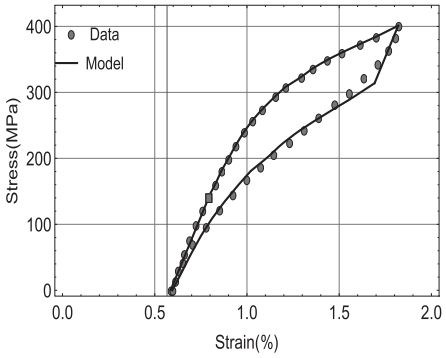


(c) 20th cycle

**Fig. 5.** Model simulations (solid lines) for the 8th, the 12th and the 20th cycle and comparisons with test data (dots) in Zaki and Moumni (2007): The irrecoverable strain becomes nearly vanishing.

stress and strain data given for each loading-unloading cycle;

(iii) Exact closed-form solutions for the uniaxial stress-stain responses of the proposed model may be obtained for any given number of loading-unloading cycles and such solutions are exactly the new single-variable shape functions in the foregoing; and, accordingly,

(iv) The new model proposed may automatically and accurately fit extensive experimental data given for any given number of loading-unloading cycles, thus bypassing uncertainties and complexities involved in usual simulation methods, as indicated in the introduction section;

(v) With the multi-axial hardening quantities $c$, $\gamma$ and $r$ identified as in Eqs. (45)–(47), the model in Section 3 is established for multi-axial cases and, therefore, responses for multi-axial loading processes can be predicted from this model, including responses for all possible uniaxial loading processes as particuoar cases.

## 6. Numerical examples for model validation

With the results presented in the last two sections, the new elastoplastic $J_2-$flow model proposed in Section 3 can automatically match test data given for any given number of uniaxial loading-unloading cycles. This may be achieved by presenting two linear functions in Eqs. (21) and (23) and suitable form of the shape functions $p_n(\overline{\tau})$ (cf., Eq. (22)) and $q_n(\underline{\tau})$ (cf., Eq. (24)). With the form of the shape function $p_n(\overline{\tau})$ given in Section 4.3, the data for the loading case may be automatically, accurately fitted. As a result, for each cycle it will suffice to present a suitable value of the parameter $b_n$ in Eq. (24) in fitting the data given for the unloading case, with the parameter $u_{0n}$ given by Eq. (27).

**Table 1**
Values of the parameter $b_n$ for seven cases of the cycle number.

| $n$ | 1 | 2 | 3 | 4 | 8 | 12 | 20 |
|---|---|---|---|---|---|---|---|
| $b_n$ | 0.250 | 0.251 | 0.382 | 0.470 | 0.602 | 0.643 | 0.701 |

For the purpose of model validation, test data for a plastic-to-pseudoelastic transition in Zaki and Moumni (2007) will be taken into consideration. In this reference, extensive data for loading and unloading curves are presented for the 1st, the 2nd, the 3rd, the 4th, the 8th, the 12th and the 20th cycle of a uniaxial SMA sample, etc. Such data show that the SMA sample tested displays a gradual transition from plastic to pseudo-elastic effects.

The value of Young's modulus is given by $E$=68GPa. Together with the linear function given in Eqs. (21) for the linear elastic part, the shape functions given in Eqs. (25)–(26) are used to automatically, exactly fit the data for the loading case at each cycle. Totally, seven such shape functions, $p_n(\overline{\tau}_n)$, are available for the seven cases at issue. Then, with these and the linear equation given in Eq. (23) for the linear elastic part, the shape functions given in Eq. (24) are used to simulate the unloading data. The values of the parameter $b_n$ are independently prescribed by Eq. (28) in fitting the unloading data for each case considered. The values of the parameter $b_n$ are listed in Table 1 for the seven cases of the cycle number, i.e., $n$=1, 2, 3, 4, 8, 12, 20.

Simulation results are depicted in Fig. 4(a)–(d) for the first four cycles and Fig. 5(a)–(c) for the 8th, 12th and 20th cycles. It may be noticeable that the loading-unloading data for each cycle may be accurately simulated by merely identifying one parameter, i.e., $b_n$. In particular, the irrecoverable strains are also simulated accurately for each cycle number at issue.

Please cite this article as: L. Zhan, X.-M. Wang and S.-Y. Wang et al., An explicit and accurate approach toward simulating plastic-to-pseudoelastic transitions of SMAs under multiple loading and unloading cycles, International Journal of Solids and Structures, https://doi.org/10.1016/j.ijsolstr.2019.08.024

## 7. Concluding remarks

In the previous sections, a new finite strain elastoplastic $J_2$−flow model with coupled hardening effects has been proposed to simultaneously simulate both plastic effects and pseudo-elastic effects of SMAs under cyclic loading conditions. The hardening quantities incorporated in this model have been presented in explicit forms, so that extensive data for any given number of loading-unloading cycles may be automatically, accurately simulated. Toward this objective, in Sections 4–5, a new approach has been proposed to combine any given number of functions over subranges into a unified, smooth function over the entire range. As such, the new approach proposed reduces the complicated problem of simulating extensive data for multiple loading cycles to presenting certain single-variable shape functions fitting such data, thus bypassing both uncertainties and complexities usually involved in iteratively resolving a coupled system of nonlinear constitutive rate equations toward identifying numerous unknown parameters.

As compared with existing models for SMA modeling, the main novelties of the new model proposed may be summarized in Section 5.6 and as follows:

(i) Continuous transitions from plastic to pseudo-elastic effects under any given number of loading-unloading cycles may be explicitly, accurately simulated for the first time;
(ii) Stress-strain data for each loading-unloading cycle are explicitly fitted by a pair of single-variable shape functions, without involving tedious numerical procedures in treating a coupled system of nonlinear constitutive rate equations incorporating a number of unknown parameters, which have to be iteratively carried out by means of the trial-and-error method in identifying numerous unknown parameters for a reasonable fit; and
(iii) Extensive loading-unloading data may be explicitly, accurately simulated by merely identifying a single parameter for each cycle, and, however, with usual approaches of SMA modeling, such data could be roughly simulated by identifying a number of unknown parameters.

It should be pointed out that the new model proposed is of phenomenological nature with no direct reference to the micro-mechanisms underlying the macroscopic behavior of SMAs. As such, it may be straightforward to simulate data for the macroscopic deformation behavior of SMA samples. A phenomenological model may be well established in the just mentioned sense and should be in no conflict with underlying micro-mechanisms. It may be noted that that would also be the case for modeling elastoplastic deformations of metals etc. Indeed, widely used phenomenological models have been well established to model macroscopic elastoplastic deformations, with no direct reference to the underlying micro-mechanisms such as dislocations and crystallographic slips, etc. However, underlying micro-mechanisms play essential roles in explaining and understanding the physical features of macroscopic deformation behaviors, as may be seen in numerous contributions in modeling deformation behaviors of SMAs, e.g., in Patoor et al. (2006) and Lagoudas et al. (2006) and the references therein.

As has been indicated in Section 4.4, the accuracy of the proposed approach in fitting test data at unloading is actually based on the consideration that both the loading and unloading curves $P_1P_2$ and $Q_1Q_2$ should be related by a linear relationship. In a broad case, that may not be the case and hence the approach proposed here could not ensure accuracy. As such, new development is needed to treat this broad case.

Results have been derived for the isothermal case with the temperature held fixed. Under different temperatures, shapes of the loading and unloading curves in Fig. 2 will temperature-dependent. The procedures proposed here may be extended to treat this non-isothermal case based on the non-isothermal framework in Xiao et al. (2011). On the other hand, It is expected that the new approach presented in this study may be extended to further simulate comprehensive effects of SMAs over the whole deformation range up to failure and, in particular, to simulate fatigue failure under cyclic and non-cyclic loadings. Results will be reported elsewhere.

## Acknowledgements

This study was supported jointly by the Talents-Introducing Project (No.: RC201703) from Ningbo Polytechnic, Ningbo, China and by the fund from NSFC (No.: 11372172), as well as the start-up fund from Jinan University, Guangzhou, China.

## References

Abeyaratne, R., Kim, S.J., 1997. Cyclic effects in shape-memory alloys: a one-dimensional continuum model. Int. J. Solids Struct. 34, 3273–3289.
Ashrafi, M.J., Arggavani, J., Naghdabadi, R., Sohrabpour, S., Auricchio, F., 2016. Theoretical and numerical modeling of dense and porous shape memory alloys accounting for coupling effects of plasticity and transformation. Int. J. Solids Struct. 88–89, 248–262.
Auricchio, F., Reali, A., Stefanelli, U., 2007. A three-dimensional model describing stress-induced solid phase transformation with permanent inelasticity. Int. J. Plast. 23, 207–226.
Baldelli, A.A.L., Maurini, C., Pham, K., 2015. A gradient approach for the macroscopic modeling of superelasticity in softening shape memory alloys. Int. J. Solids Struct. 52, 45–55.
Bo, Z., Lagoudas, D., 1999a. Thermomechanical modeling of polycrystalline SMAs under cyclic loading, part i: theoretical derivations. Int. J. Eng. Sci. 37, 1089–1104.
Bo, Z., Lagoudas, D., 1999b. Thermomechanical modeling of polycrystalline SMAs under cyclic loading, part iii: evolution of plastic strains and two-way shape memory effect. Int. J. Eng. Sci. 37, 1175–1203.
Bo, Z., Lagoudas, D., 1999c. Thermomechanical modeling of polycrystalline SMAs under cyclic loading, part iv: modeling of minor hysteresis loops. Int. J. Eng. Sci. 37, 1205–1249.
Bruhns, O.T., Xiao, H., Meyers, A., 2003. Some basic issues in traditional Eulerian formulations of finite elastoplasticity. Int. J. Plast. 19, 2007–2026.
Bruhns, O.T., Xiao, H., Meyers, A., 2005. A weakened form of Ilyushin's postulate and the structure of self-consistent Eulerian finite elastoplasticity. Int. J. Plast. 21, 199–219.
Cui, S., Wan, J., Zuo, X., Chen, N., Zhang, J., Rong, Y., 2017. Three-dimensional non-isothermal phase-field modeling of thermally and stress-induced martensitic transformations in shape memory alloys. Int. J. Solids Struct. 109, 1–11.
Dong, L., Zhou, R.H., Wang, X.L., Hu, G.K., Sun, Q.P., 2016. On interfacial energy of macroscopic domains in polycrystalline NiTi shape memory alloys. Int. J. Solids Struct. 80, 445–455.
Hartl, D.J., Chatzigeorgiou, P., Lagoudas, D.C., 2010. Three-dimensional modeling and numerical analysis of rate-dependent irrecoverable deformation in shape memory alloys. Int. J. Plast. 26, 1485–1507.
Hartl, D.J., Kiefer, B., Schulte, R., Menzel, A., 2018. Computationally-efficient modeling of inelastic single crystal responses via anisotropic yield surface: applications to shape memory alloys. Int. J. Solids Struct. 136, 38–59.
Hartl, D.J., Lagoudas, D.C., 2009. Constitutive modeling and structural analysis considering simultaneous phase transformation and plastic yield in shape memory alloys. Smart Mater. Struct. 18, 104017–104033.
Jiang, D.J., Bechle, N.J., Landis, C.M., Kyriakides, S., 2016a. Buckling and recovery of NiTi tubes under axial compression. Int. J. Solids Struct. 80, 52–63.
Jiang, D.J., Landis, C.M., Kyriakides, S., 2016b. Effects of tension/compression asymmetry on the buckling and recovery of NiTi tubes under axial compression. Int. J. Solids Struct. 100, 41–53.
Lagoudas, D., Bo, Z., 1999. Thermomechanical modeling of polycrystalline SMAs under cyclic loading, part ii: material characterization and experimental results for a stable transformation cycle. Int. J. Eng. Sci. 37, 1141–1173.
Lagoudas, D.C., 2008. Shape Memory Alloys: Modeling and Engineering Applications. Springer, New York.
Lagoudas, D.C., Entchev, P.B., Popov, P., Patoor, E., Brinson, L.C., Gao, X., 2006. Shape memory alloys, part ii: modeling of polycrystals. Mech. Mater. 38, 430–462.
Lagoudas, D.C., Hartl, D., Chemisky, Y., Machado, L., Popov, P., 2012. Constitutive model for the numerical analysis of phase transformation in polycrystalline shape memory alloys. Int. J. Plast. 32, 155–183.
Luig, P., Bruhns, O.T., 2008. On the modeling of shape memory alloys using tensorial internal variables. Mat. Sci. Eng. A 481–482, 379–383.
Morin, C., Moumni, Z., Zaki, W., 2011a. Thermomechanical coupling in shape memory alloys under cyclic loadings: experimental analysis and constitutive modelling. Int. J. Plast. 27, 1959–1980.
Morin, C., Moumni, Z., Zaki, W., 2011b. A constitutive model for shape memory alloys accounting for thermomechanical coupling. Int. J. Plast. 27, 748–767.

Please cite this article as: L. Zhan, X.-M. Wang and S.-Y. Wang et al., An explicit and accurate approach toward simulating plastic-to-pseudoelastic transitions of SMAs under multiple loading and unloading cycles, International Journal of Solids and Structures, https://doi.org/10.1016/j.ijsolstr.2019.08.024

Panico, M., Brinson, L.C., 2007. A three-dimensional phenomenological model for martensite reorientation in shape memory alloys. J. Mech. Phys. Solids 55, 2491–2511.
Patoor, E., Lagoudas, D.C., Entchev, P., Brinson, L.C., Gao, X., 2006. Shape memory alloys, part i: general properties and modeling of single crystals. Mech. Mater. 38, 391–429.
Saint-Sulpice, L., Chirani, S.A., Calloch, S., 2009. A 3d super-elastic model for shape memory alloys taking into account progressive strain under cyclic loadings. Mech. Mater. 41, 12–26.
Shaw, J.A., Kyriakides, S., 1995. Thermomechanical aspects of NiTi. J. Mech. Phys. Solids 43, 1243–1281.
Tanaka, K., Nishimura, F., Hayashi, T., Tobushi, H., Lexcellent, C., 1995. Phenomenological analysis on subloops and cyclic behavior in shape memory alloys under mechanical and/or thermal loads. Mech. Mater. 19, 281–292.
Wang, X.M., Wang, Z.L., Xiao, H., 2015. SMA pseudo-elastic hysteresis with tension–compression asymmetry:explicit simulation based on elasticity models. Continuum Mech. Thermodyn. 27, 959–970.
Xiao, H., 2013. Pseudo-elastic hysteresis out of recoverable finite elastoplastic flows. Int. J. Plast. 41, 82–96.
Xiao, H., 2014a. An explicit,straightforward approach to modeling SMA pseudo-elastic hysteresis. Int. J. Plast. 53, 228–240.
Xiao, H., 2014b. Thermo-coupled elastoplasticity model with asymptotic loss of the material strength. Int. J. Plast. 63, 211–228.
Xiao, H., Bruhns, O.T., Meyers, A., 1997a. Logarithmic strain,logarithmic spin and logarithmic rate. Acta Mech. 124, 89–105.
Xiao, H., Bruhns, O.T., Meyers, A., 1997b. Strain rates and material spins. J. Elast. 52, 1–41.
Xiao, H., Bruhns, O.T., Meyers, A., 1997c. On objective corotational rates and their defining spin tensors. Int. J. Solids Struct. 35, 4001–4014.
Xiao, H., Bruhns, O.T., Meyers, A., 2000a. The choice of objective rates in finite elastoplasticity: general results on the uniqueness of the logarithmic rate. Proc. Roy. Soc. London A 456, 1865–1882.
Xiao, H., Bruhns, O.T., Meyers, A., 2000b. A consistent finite elastoplasticity theory combining additive and multiplicative decomposition of the stretching and the deformation gradient. Int. J. Plast. 16, 143–177.
Xiao, H., Bruhns, O.T., Meyers, A., 2006. Elastoplasticity beyond small deformations. Acta Mech. 182, 31–111.
Xiao, H., Bruhns, O.T., Meyers, A., 2007. Thermodynamic laws and consistent Eulerian formulations of finite elastoplasticity with thermal effects. J. Mech. Phys. Solids 55, 338–365.
Xiao, H., Bruhns, O.T., Meyers, A., 2010a. Finite elastoplastic $j_2$−flow models with strain recovery effects. Acta Mech. 210, 13–25.
Xiao, H., Bruhns, O.T., Meyers, A., 2010b. Phenomenological elastoplasticity view on strain recovery loops characterizing shape memory materials. ZAMM-J. Appl. Math. Mech. 90, 544–564.
Xiao, H., Bruhns, O.T., Meyers, A., 2011. Thermo-induced plastic flows and shape memory effects. Theor. Appl. Mech. 38, 155–207.
Xiao, H., Wang, X.M., Wang, Z.L., Yin, Z.N., 2016. Explicit, comprehensive modeling of multi-axial finite strain pseudo-elastic SMAs up to failure. Int. J. Solids Structures 88–89, 215–226.
Zaki, W., Moumni, Z., 2007. A 3d model of the cyclic thermomechanical behavior of shape memory alloys. J. Mech. Phys. Solids 55, 2427–2454.
Zhou, B., 2012. A macroscopic constitutive model of shape memory alloy considering plasticity. Mech. Mater. 48, 71–81.

Please cite this article as: L. Zhan, X.-M. Wang and S.-Y. Wang et al., An explicit and accurate approach toward simulating plastic-to-pseudoelastic transitions of SMAs under multiple loading and unloading cycles, International Journal of Solids and Structures, https://doi.org/10.1016/j.ijsolstr.2019.08.024